Studies of the Enzymic Mechanism of *Candida tenuis* Xylose Reductase (AKR 2B5): X-ray Structure and Catalytic Reaction Profile for the H113A Mutant[†,‡]

Regina Kratzer,[§] Kathryn L. Kavanagh,[||] David K. Wilson,[||] and Bernd Nidetzky*[,§]

Institute of Biotechnology, Graz University of Technology, Petersgasse 12/I, A-8010 Graz, Austria, and Section of Molecular and Cellular Biology, University of California, Davis, California 95616

Received October 10, 2003; Revised Manuscript Received February 10, 2004

ABSTRACT: Xylose reductase from the yeast *Candida tenuis* (CtXR) is a family 2 member of the aldo−keto reductase (AKR) superfamily of proteins and enzymes. Active site His-113 is conserved among AKRs, but a unified mechanism of how it affects catalytic activity is outstanding. We have replaced His-113 by alanine using site-directed mutagenesis, determined a 2.2 Å structure of H113A mutant bound to $NADP^+$, and compared catalytic reaction profiles of NADH-dependent reduction of different aldehydes catalyzed by the wild type and the mutant. Deuterium kinetic isotope effects (KIEs) on k_{cat} and $k_{cat}/K_{m\ xylose}$ show that, relative to the wild type, the hydride transfer rate constant ($k_7 \approx 0.16\ s^{-1}$) has decreased about 1000-fold in H113A whereas xylose binding was not strongly affected. No solvent isotope effect was seen on k_{cat} and $k_{cat}/K_{m\ xylose}$ for H113A, suggesting that proton transfer has not become rate-limiting as a result of the mutation. The pH profiles of $\log(k_{cat}/K_{m\ xylose})$ for the wild type and H113A decreased above apparent pK_a values of 8.85 and 7.63, respectively. The ΔpK_a of −1.2 pH units likely reflects a proximally disruptive character of the mutation, affecting the position of Asp-50. A steady-state kinetic analysis for H113A-catalyzed reduction of a homologous series of meta-substituted benzaldehyde derivatives was carried out, and quantitative structure−reactivity correlations were used to factor the observed kinetic substituent effect on k_{cat} and $k_{cat}/K_{m\ aldehyde}$ into an electronic effect and bonding effects (which are lacking in the wild type). Using the Hammett σ scale, electronic parameter coefficients (ρ) of +0.64 (k_{cat}) and +0.78 ($k_{cat}/K_{m\ aldehyde}$) were calculated and clearly differ from $\rho(k_{cat}/K_{aldehyde})$ and $\rho(k_{cat})$ values of +1.67 and approximately 0.0, respectively, for the wild-type enzyme. Hydride transfer rate constants of H113A, calculated from kinetic parameters and KIE data, display a substituent dependence not seen in the corresponding wild-type enzyme rate constants. An enzymic mechanism is proposed in which His-113, through a hydrogen bond from Nϵ2 to aldehyde O1, assists in catalysis by optimizing the C═O bond charge separation and orbital alignment in the ternary complex.

The aldo−keto reductases (AKRs)[1] constitute a large protein superfamily and are widespread in nature (*1*). They all seem to bind to NAD(P) and with few exceptions display NAD(P)-dependent oxidoreductase activity (*1*, *2*). AKRs are single-domain proteins of ≈36 kDa mass and share a common $(\beta/\alpha)_8$ barrel fold. The canonical active site conformation of AKRs involves a tetrad of Tyr-51, Lys-80, Asp-46, and His-113 [numbered according to CtXR (*3*); Figure 1A] (*2*). In a multiple sequence alignment across all current 14 AKR families, the positions of the tetrad residues are highly conserved, suggesting a common mechanistic basis of catalytic action (*1*).

An enzymic mechanism for AKRs has been suggested which assigns roles in catalysis to Tyr-51, Lys-80, and Asp-46 (*4*−*10*). Tyr-51 is widely believed to function as the general acid/base catalyst of the reaction (*4*−*10*). The $-NH_2$ group of Lys-80 is protonated under the physiological pH conditions and brought into position through a salt link interaction with the carboxylate side chain of Asp-46. It is thought to donate a hydrogen for bonding with a lone electron pair on the oxygen of the phenolic hydroxyl of the tyrosine. The pK_a of Tyr-OH is thus depressed from a value of ≈10.5 in aqueous solution to a value between about 7 and 9 in both the enzyme−NADPH complex (*6*−*8*, *11*) and the ternary complex (*4*, *5*). The pK_a shift by ≥1.5 pH units is required for Tyr-51 to function as an effective proton donor

[†] Financial support is acknowledged from the Austrian Science Funds (P-15208-MOB to B.N.), the National Institutes of Health (D.K.W.), and the Keck Foundation. K.L.K. is supported by a grant from the University of California Systemwide Biotechnology Research Program, proposal number 2001-07. The data collection facilities at Stanford Synchrotron Radiation Laboratory are funded by the U.S. Department of Energy and by the National Institutes of Health.

[‡] The coordinates and structure factors for the H113A mutant of *C. tenuis* xylose reductase have been deposited into the Protein Data Bank under the accession number 1R38. Coordinates are numbered according to the DNA sequence with the initiator methionine as residue 1. Numbering within this paper follows the convention of the mature protein in which the initial methionine is processed off; hence residue numbers differ by one.

* Corresponding author. Phone: +43-316-873-8400. Fax: +43-316-873-8434. E-mail: bernd.nidetzky@tugraz.at.

[§] Graz University of Technology.

[||] University of California.

[1] Abbreviations: AKR, aldo−keto reductase; AR, aldose reductase; hAR, human AR; XR, xylose reductase [alditol:$NAD(P)^+$ 1-oxidoreductase; EC 1.1.1.21]; CtXR, XR from *Candida tenuis*; BA, benzaldehyde; 3X-BA, BA substituted in the meta position on the aromatic ring; 3X-BzOH, substituted benzyl alcohol; KIE, kinetic isotope effect; S-KIE, solvent kinetic isotope effect.

10.1021/bi035833r CCC: $27.50
Published on Web 04/07/2004

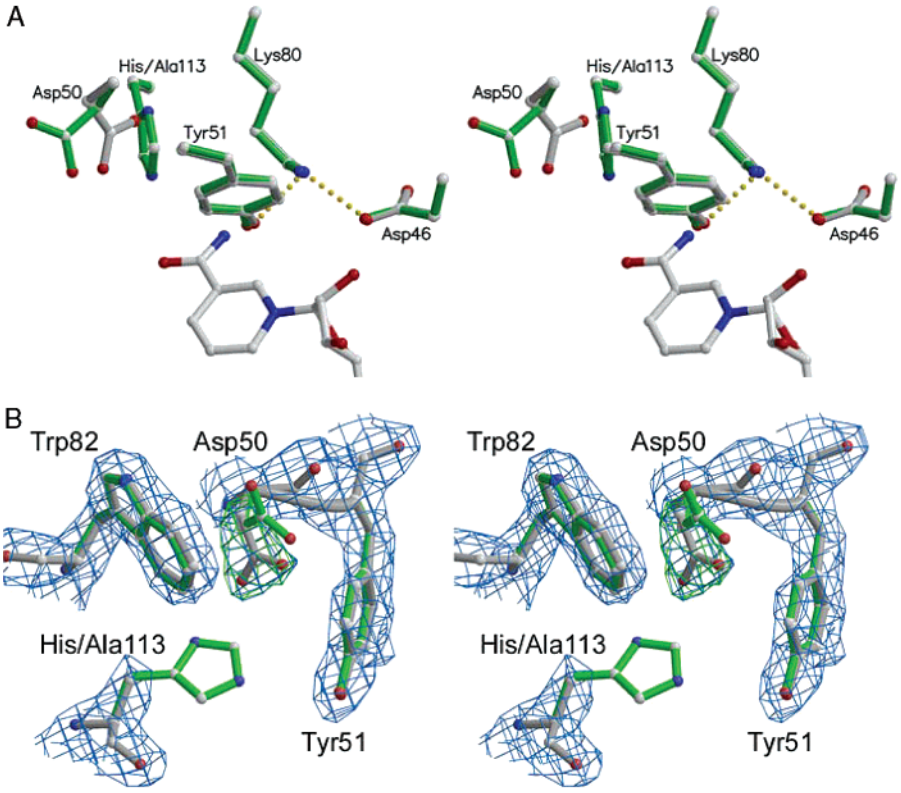

FIGURE 1: (A) Overlap of wild-type CtXR (green bonds) and H113A (gray bonds) that includes the nicotinamide from the mutant structure. Hydrogen bonds between catalytically important residues are depicted as gold dotted lines. (B) Representative $2F_o - F_c$ (blue; contoured at 1.4σ) and $F_o - F_c$ (green; contoured at 6σ) electron density. Phases were calculated from the final refined H113A model with the side-chain atoms of Asp-50 omitted. Side chains are colored as in panel A.

for carbonyl group reduction. Characterization of CtXR mutants Y51F and K80A yielded results supporting these basic components of the AKR catalytic mechanism (*12*).

The question of the exact role of His-113 has been a topic of controversy over the years. Site-directed replacements of His-113 by Asn, Gln, Glu, or Ala in different AKRs gave mutant enzymes that displayed low, however, robust activity (*4*−*11*), indicating an auxiliary function for the histidine in the AKR catalytic mechanism. Analysis of kinetic consequences of the mutations using comparative pH and isotope effect studies led to consideration of different mechanistic proposals. First, His-113 is required for substrate orientation in the binding pocket (*6*, *8*, *11*), likely by donating a hydrogen for bonding from the Nϵ2−H of its neutral imidazole ring. Second, it assists in proton transfer from Tyr-OH to the oxygen atom of the reactive carbonyl group in the reductive direction of the reaction (*4*, *5*, *11*). In this scenario, the side chain of His-113 is doubly protonated at the optimum pH for reduction. A number of computational studies have suggested, however, that formation of a positively charged imidazolium ring is energetically disfavored at AKR active sites (*13*, *14*), although this notion is not without criticism (*15*). Penning and co-workers argue that the delocalized positive charge on the imidazole ring is part of a catalytic proton relay between His-113 and Tyr-51 that facilitates carbonyl group reduction (*4*, *5*, *11*). Considering the available evidence from previous experimental and theoretical investigations, neither of the two mechanisms for His-113 is ultimately persuasive, and a unified description of how His-113 affects AKR catalytic activity is still outstanding.

The present paper describes experiments that were designed to explore the role of His-113 in the NADH-dependent reduction of aldehydes by CtXR. We report enzyme kinetics and the X-ray structure of a H113A mutant and show that, in CtXR, His-113 facilitates the reaction through the precise positioning of the substrate carbonyl group at the active site. This mechanism explains the high conservation of the histidine throughout the superfamily, and we will discuss that it is consistent with observations made by others with different AKRs.

MATERIALS AND METHODS

Materials. All chemicals and reagents have been described elsewhere (*16*).

Mutagenesis, Enzyme Production, and Purification. An inverse PCR method was employed to mutate His-113 into alanine (*17*). The mutagenic oligonucleotide primers used are listed below with the mismatched bases underlined: H113A (forward), 5′-GTTCTTGATCGCTTTCCCAATTG-3′; H113A (reverse), 5′-AAGTCAACGTAGTCAACCT-TAAG-3′. Plasmid miniprep DNA was subjected to dideoxy sequencing to verify the introduction of the desired mutations and that no misincorporations of nucleotides had occurred because of DNA polymerase errors. Expression of the mutagenized gene in *Escherichia coli* was carried out by reported methods (*18*). SDS−PAGE analysis of induced and noninduced cell extracts was used to confirm the synthesis of the recombinant protein. H113A was purified by Red 31 dye ligand chromatography (*18*). MonoQ anion-exchange chromatography that is used as the polishing step in the purification of the wild-type enzyme (*18*) was omitted

Table 1: Summary of H113A CtXR Data Collection, Refinement, and Models

Data Collection	
space group	*C*2
unit cell	
a (Å)	179.98
b (Å)	129.09
c (Å)	79.87
β (deg)	90.82
monomers per asymmetric unit	4
resolution range (Å)	30−2.2 (2.24−2.2)
no. of observations/unique reflections	306084/93679
R_{merge} (overall/high-resolution shell)	0.074/0.294
completeness (overall/high-resolution shell) (%)	99.4/100
$I/\sigma(I)$ (overall/high-resolution shell)	15.3/3.9
Model	
protein atoms	10108
$NADP^+$ atoms	192
water molecules	827
Refinement	
reflections used ($I > 0$)	91,348
R_{cryst}	0.185
R_{free}	0.226
rmsd from ideal bond length (Å)	0.011
rmsd from ideal bond angle (deg)	1.50

because the mutant precipitated on the column. Therefore, only the peak fractions of H113A eluting from the dye column collection were used further. The H113A preparation was electrophoretically pure (see Supporting Information). Protein concentrations were determined with the BCA protein assay (Pierce) using BSA as the reference.

Crystallization and Structure Determination. Crystals of the mutant holoenzyme were obtained using the vapor diffusion technique in conditions similar to those of the wild type. The protein stock solution used for crystallization was 17 mg/mL mutant protein in 10 mM Hepes and 3 mM $NADP^+$, pH 7.4. A drop composed of 2 μL of protein solution and 1 μL of well solution was suspended over a well containing 0.35 M ammonium sulfate, 32% (w/v) poly(ethylene glycol) methyl ether 5000, and 100 mM citrate, pH 5.6. These were harvested into a cryoprotectant containing 75% well solution and 25% ethylene glycol and flash cooled prior to data collection.

Diffraction data were collected on a Mar Research 345 imaging plate detector mounted on beamline 7-1 at Stanford Synchrotron Radiation Laboratory (SSRL). The crystals were indexed, and reflections were integrated using DENZO (*19*). Data were merged using SCALEPACK, yielding a 2.2 Å data set with an R_{merge} of 7.4%. Other relevant data collection statistics are given in Table 1.

The structure of the mutant was determined using molecular replacement as implemented by EPMR (*20*). The search object was the dimer of the wild-type apoenzyme [PDB accession code 1JEZ (*21*)] and was used to locate the two dimers that compose the asymmetric unit. A correlation coefficient of 0.56 and a crystallographic *R*-factor of 41.5% were observed for the initial model. Alternating cycles of manual refitting using O (*22*) and crystallographic refinement using CNS (*23*) were used to produce the final model. Final statistics describing the refinement and model quality are given in Table 1.

3F-BA Modeling. Polar hydrogens were added to the crystal structures, and molecules of *m*-fluorobenzaldehyde (3F-BA) were manually placed into the active site of wild-type CtXR and H113A holoenzymes. Resultant structures were energy minimized for 100 steps using the program CNS (*23*). The final models were analyzed for substrate orientation conducive to catalysis as well as potential polar and hydrophobic interactions.

Steady-State Enzyme Kinetics and Ligand Binding. All experiments were carried out in 50 mM potassium phosphate buffer, pH 7.0, and at 25 °C unless otherwise mentioned. Initial rates of aldehyde reduction or alcohol oxidation by H113A and the wild-type enzyme were measured with a Beckman DU-800 spectrophotometer monitoring the consumption and formation of NAD(P)H. Typical reaction mixtures contained a concentration of H113A in the range 0.5−11.5 μM, which is between 10- and 1000-fold above the corresponding wild-type enzyme levels used. Time courses of H113A-catalyzed reactions were monitored for ≥15 min, compared to ≤5 min for the wild-type enzyme. Other methods of the initial rate analysis have been reported elsewhere (*16*).

Apparent dissociation constants ($K_{d\ NAD(P)}$) of the wild-type enzyme and H113A complexes with $NAD(P)^+$ were determined by fluorescence titration. Quenching of tryptophan fluorescence (excitation 295 nm, emission 340 nm) upon the addition of $NADP^+$ to a solution of the wild-type enzyme or H113A (3−5 μM) served as a reporter of binding and was recorded with a Hitachi F-4500 fluorescence spectrophotometer equipped with a temperature-controlled cell holder. Typically, 2−4 μL aliquots of the stock solution of NAD^+ (2 mM) or $NADP^+$ (0.1 mM) were added incrementally to yield a final nucleotide level of $>6K_d$.

pH and Kinetic Isotope Effects. Studies of pH effects on the catalytic rates of the wild-type enzyme and H113A in the direction of NADH-dependent reduction of xylose were carried out at 25 °C in potassium phosphate buffer (pH range 6.0−8.0) and Tris-HCl buffer (pH range 8.0−9.0) at a constant value of $I = 0.02$ for the molar ionic strength. Initial rates were obtained under conditions in which [xylose] was varied and [coenzyme] was constant and saturating ($>5K_{m\ NAD(P)H}$; 230 μM). Suitable control experiments showed that the wild-type enzyme and mutant were stable in the chosen pH range over the time of the assays. Primary deuterium kinetic isotope effects (KIEs) and solvent KIEs (S-KIEs) on apparent kinetic parameters of aldehyde reduction by the wild-type enzyme and H113A were obtained under conditions described elsewhere in detail (*16*).

Data Processing. Kinetic parameters or ligand binding constants were obtained from unweighted nonlinear least-squares fits of experimental data to eqs 1−8 using the program Sigmaplot 2001 (for Windows, version 7.0). Initial rate data yielding linear Lineweaver−Burk plots were fitted to the equation

$$v = k_{cat}[E][A]/(K_{m\ A} + [A]) \quad (1)$$

where v is the initial rate, [E] is the molar concentration of the enzyme subunit (36 kDa), [A] is the substrate or coenzyme concentration, k_{cat} is the turnover number (s^{-1}), and $K_{m\ A}$ is an apparent Michaelis−Menten constant. Unless otherwise stated, estimates of kinetic parameters had standard errors of <10%.

pH profiles that were level below pK_a and decreased above pK_a with a slope of −1 were fitted to eq 2. pH profiles

displaying a constant value at high (C_H) and low pH (C_L) were fitted to eq 3. In eqs 2 and 3, Y is k_{cat} or $k_{cat}/K_{m\ xylose}$,

$$\log Y = \log[C/(1 + K_a/[H^+])] \quad (2)$$

$$\log Y = \log[(C_L + C_H K_a/[H^+])/(1 + K_a/[H^+])] \quad (3)$$

C is the pH-independent value of Y, K_a is a macroscopic dissociation constant, and $[H^+]$ is the proton concentration.

KIEs or S-KIEs on steady-state kinetic parameters were calculated from fits to eq 4 of initial rate data recorded with

$$v = k_{cat}[E][A]/\{K_{m\ A}(1 + FE_{V/K}) + [A](1 + FE_V)\} \quad (4)$$

unlabeled and deuterium-labeled substrate or solvent. In eq 4, E_V and $E_{V/K}$ are the isotope effects minus 1 on k_{cat} and k_{cat}/K_m, respectively, and F is the fraction of deuterium label in the substrate or the solvent. Equations 5 and 6 were used

$$K_{d\ Ald} = K_m[^D(k_{cat}/K_m) - 1]/(^Dk_{cat} - 1) \quad (5)$$

$$k_7 = k_{cat}(^Dk_7 - 1)/(^Dk_{cat} - 1) \quad (6)$$

to obtain estimates for dissociation constants of central enzyme−NADH−aldehyde complexes ($K_{d\ Ald}$) (*24*) and the rate constant of hydride transfer from NADH (k_7) (*25*), respectively. $^D(k_{cat}/K_m)$ and $^Dk_{cat}$ are KIEs on k_{cat} and k_{cat}/K_m. $^Dk_7$ is an intrinsic KIE on k_7 and is assumed to have a value of ≈6.5 (*26*).

Data from fluorescence titration with $NAD(P)^+$ were fitted to the equation

$$[E]_{bound} = [E]_{tot}[NAD(P)^+]_{free}/(K_{d\ NAP(P)^+} + [NAD(P)^+]_{free}) \quad (7)$$

where $[E]_{bound}$ is the fractional saturation multiplied by the molar concentration of the enzyme subunit ($[E]_{tot}$; 36 kDa), $[NAD(P)^+]_{free}$ is the concentrated of unbound coenzyme, and $K_{d\ NAD(P)^+}$ is an apparent dissociation constant. Under conditions in which $[E]_{tot} \approx K_{d\ NAD(P)^+}$, $[NAD(P)^+]_{free}$ is significantly smaller than the total concentration of added coenzyme $[NAD(P)^+]_{tot}$. Therefore, eq 8 was used to fit fluorescence quenching data:

$$[E]_{bound} = \{(K_{d\ NAP(P)^+} + [E]_{tot} + [NAD(P)^+]_{tot}) - [(K_{d\ NAP(P)^+} + [E]_{tot} + [NAD(P)^+]_{tot})^2 - 4[E]_{tot}[NAD(P)^+]_{tot}]^{1/2}\}/2 \quad (8)$$

RESULTS

X-ray Structure of the H113A Mutant. As previously observed in the wild-type CtXR holoenzyme structure, there are four monomers (two dimers) in the asymmetric unit for the H113A holoenzyme. Root mean square differences between the monomers are less than 0.35 and 0.6 Å for α carbons and all atoms, respectively. The structure of H113A bound to $NADP^+$ is highly homologous to the wild-type XR−$NADP^+$ binary complex, with the $NADP^+$ binding in a conformation identical to that of the wild type and making similar interactions. When comparing monomer B of the wild-type enzyme to monomer D of the mutant structure, root mean square deviations between α carbons and all atoms are 0.13 and 0.41 Å, respectively. As these two subunits have the lowest temperature factors in their respective asymmetric units, they were used as reference molecules for structural comparisons and modeling. The most significant structural difference occurs in the side chain of Asp-50.

The density and temperature factors for the Asp-50 side chain suggest that it may be more mobile in H113A. In monomers A, B, and C of the wild-type enzyme, temperature factors of all the atoms in the Asp-50 side chain are ≈23 Å^2. Asp-50 of the wild-type monomer D has higher temperature factors (28−34 Å^2); nevertheless, the electron density is unambiguous and indicates a single conformation. For H113A, the β carbons of Asp-50 have temperature factors of 23−27 Å^2, but the carboxylate atoms have values ranging from 31 to 41 Å^2, indicating greater positional disorder. The predominant conformation has the carboxylate rotated down toward where the His-113 imidazole was located. When monomer B of the wild-type enzyme is overlaid onto monomer D of H113A, the distance from the mutant Asp-50 Oδ1 to wild-type His-113 Cϵ1 is 2.12 Å. Hence, the primary conformation of Asp-50 in H113A would be sterically excluded in the wild-type enzyme. A conformation with lower occupancy is similar to what is observed in wild-type CtXR. The carboxylate of Asp-50 is held roughly parallel to the Trp-82 side chain in both instances as shown in Figure 1B. Although the resolution of the data prohibited refining alternate conformations for this side chain, electron density suggests approximately 75% in the major conformation. This places the Asp-50 carboxylate ≈5 Å from the tyrosine hydroxyl, closer than the ≈6.5 Å in wild-type CtXR but not as close as the ≈4 Å His-to-Tyr distance observed in the wild type.

Energy-Minimized Models of 3F-BA Binding. m-Fluorobenzaldehyde can be modeled into the active site in one of two productive orientations (Figure 2). Both orientations have the carbonyl carbon above the NADH C4 and the carbonyl oxygen within hydrogen bond distance of the tyrosine hydroxyl. In wild-type CtXR, the oxygen is held in place by an additional polar interaction with His-113. This interaction is obviously lacking in H113A, and there is more variability in the oxygen position. For both the wild-type enzyme and H113A the fluorine can be directed either into a hydrophobic pocket or toward bulk solvent.

Kinetic Properties of the H113A Mutant Compared to the Wild-Type Enzyme. Steady-state kinetic parameters for NAD(P)H-dependent reduction of xylose and NAD^+-dependent oxidation of xylitol catalyzed by H113A and the wild-type enzyme were determined and are compared in Table 2. Apparent dissociation constants of binary enzyme−$NAD(P)^+$ complexes were obtained from fluorescence titration data and are also shown in Table 2. The values of $K_{d\ NAD(P)^+}$ and the apparent Michaelis constants for NAD(P)H were not changed much (≤5-fold) as a result of the mutation. However, turnover number and catalytic efficiency for reaction with substrate in the presence of a saturating coenzyme concentration were between 500- and 1000-fold decreased in H113A. The loss of catalytic proficiency (k_{cat}/K_m) of the mutant, compared to the wild-type enzyme, was identical within experimental error in the forward and reverse directions of the reaction. Since K_m values of the wild-type enzyme and H113A for the substrates xylose and xylitol were very similar, the observed decreases

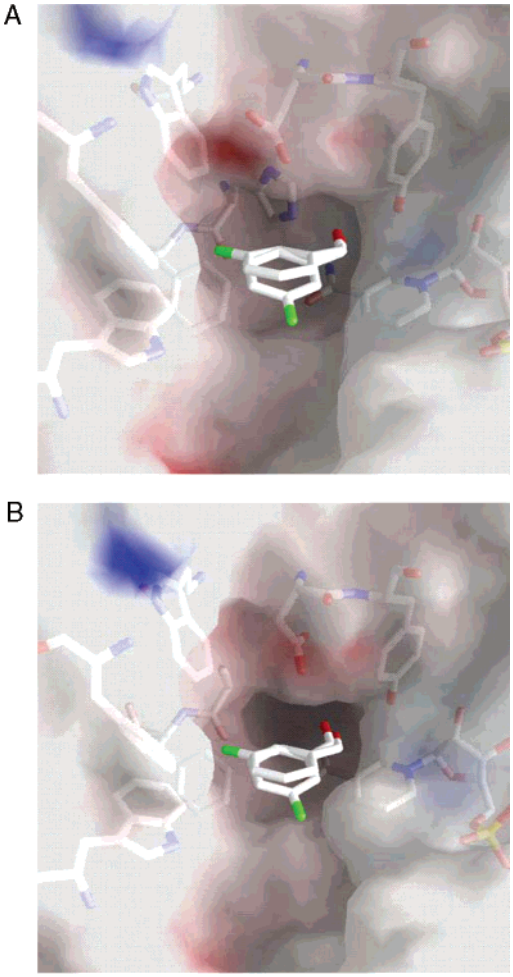

FIGURE 2: (A) Surface representation of the wild-type CtXR active site with energy-minimized structures of *m*-fluorobenzaldehyde. Asp-50, Tyr-51, His-113, NADH, and residues forming the hydrophobic pocket are shown beneath the transparent surface. (B) Surface representation of H113A with energy-minimized structures of *m*-fluorobenzaldehyde. Surfaces in (A) and (B) are colored by electrostatic potential, and the fluorine is colored green. The figures were created using the programs MolScript (*25*), Bobscript (*26*), Raster3D (*27*), and Grasp (*28*).

Table 2: Apparent Kinetic Parameters for Xylose Reduction and Xylitol Oxidation Catalyzed by Wild-Type CtXR and H113A Mutant

parameter	wild type	H113A
$k_{cat\ red}$ (s^{-1})[a]	12.4 (18.9)[b]	0.024 (0.12)[b]
$K_{m\ xylose}$ (mM)	91 (78)[b]	123 (391)[b]
$k_{cat\ red}/K_{m\ xylose}$ ($M^{-1}\ s^{-1}$)	136 (241)[b]	0.19 (0.32)[b]
$K_{m\ NAD(P)H}$ (μM)[c]	39 (3.2)[b]	34 (2.8)[b]
$k_{cat\ ox}$ (s^{-1})[a]	1.1	9×10^{-4}
$K_{m\ xylitol}$ (mM)	334	452
$k_{cat\ ox}/K_{m\ xylitol}$ ($M^{-1}\ s^{-1}$)	3.3	0.0021
$K_{d\ NAD(P)^+}$ (μM)[d]	188[e,g] (1.3)[f,g]	72[e,g] (0.84)[f,g]

[a] $k_{cat\ red}$ and $k_{cat\ ox}$ are turnover numbers in the directions of xylose reduction and xylitol oxidation, respectively. [b] Values in parentheses were obtained with NADPH. [c] [Xylose] matching $K_{m\ xylose}$ was used. [d] Values in parentheses were obtained with $NADP^+$. [e] From fits of data from fluorescence titrations with NAD^+ to eq 7. [f] From fits of data from fluorescence titrations with $NADP^+$ to eq 8. [g] Standard errors were <15%.

in k_{cat}/K_m for the mutant result from decreases in the value of k_{cat} by about the same factor. Like the wild-type enzyme, H113A showed an ≈2-fold greater catalytic efficiency for xylose reduction by NADPH than NADH. k_{cat} values for H113A were ≈5.5-fold higher with NADPH than NADH. By contrast, the wild-type enzyme used NADPH and NADH at similar turnover numbers. Rate-limiting steps for k_{cat} are clearly different for xylose reductions catalyzed by the wild-type enzyme and H113A (see below), explaining a ratio of NADPH- and NADH-dependent turnover numbers that is greater for H113A than the wild-type enzyme.

Table 3: Apparent Kinetic Parameters for NADH-Dependent Reduction of Aldehydes Differing in the Substituent at C2, Catalyzed by Wild-Type CtXR and the H113A Mutant

	wild type			H113A		
substrate	k_{cat} (s^{-1})	k_{cat}/K_m ($M^{-1}\ s^{-1}$)	$\Delta\Delta G^{\ddagger}$[a] (kJ/mol)	k_{cat} (s^{-1})	k_{cat}/K_m ($M^{-1}\ s^{-1}$)	$\Delta\Delta G^{\ddagger}$[a] (kJ/mol)
propanal	5.3	34		0.014	0.22	
methylglyoxal	10.8	1520	−9.4	0.083	11.1	−9.8
D-galactose	10.9	52		0.016	0.056	
2-deoxy-D-galactose		2.8[b]	7.2		0.0022[b]	8.0

[a] Calculated by using the relationship $\Delta\Delta G^{\ddagger} = -RT \ln [(k_{cat}/K_{m\ C2\ derivative})/(k_{cat}/K_{m\ parent})]$. [b] Because saturation in the substrate was not achieved, k_{cat}/K_m was determined from the linear part of the Michaelis−Menten curve.

Effect of the Substituent at the α Carbon of the Aldehyde Substrate. We carried out a steady-state kinetic analysis for NADH-dependent reduction of a series of aldehydes differing in the substituent at the α carbon atom. Kinetic parameters for the wild-type enzyme and H113A are summarized in Table 3. Comparison of k_{cat}/K_m values reveals that the α-carbonyl group of methylglyoxal, compared to the methylene group of propanal, makes a significant contribution to specificity, which was similar in the wild-type enzyme and H113A. Replacement of the C2(*R*) hydroxy group in D-galactose by a hydrogen caused identical decreases in k_{cat}/K_m for reactions catalyzed by the wild-type enzyme and H113A. We conclude, therefore, that mutation of His-113 does not bring about significant changes, compared to the wild-type enzyme, regarding the effect of the α carbon substituent on k_{cat}/K_m.

pH Effects on Kinetic Parameters for Xylose Reduction. Kinetic parameters for NADH-dependent xylose reduction by the wild-type enzyme and H113A mutant were obtained in the pH range 6.0−9.0. pH profiles of $\log(k_{cat}/K_m)$ and $\log k_{cat}$ are shown in panels A and B of Figure 3, respectively. The pH profiles in Figure 3A are level below pK_a and decrease with −1 slope above pK_a. The data were fitted to eq 2, and pK_a values of 8.85 ± 0.26 and 7.63 ± 0.06 have been calculated for the wild type and H113A, respectively. The pH profile of $\log k_{cat}$ for the wild type was a wave. A fit of the data to eq 3 gave a pK_a of 7.80 ± 0.07. The pH dependence of $\log k_{cat}$ for xylose reduction by H113A was not significant in the pH range examined.

Kinetic Isotope Effects. Initial rates of xylose reduction were recorded using NADH or NADD as the coenzyme. They were obtained under conditions in which [substrate] was varied and [coenzyme] was constant and saturating (230 μM). Data were fitted to eq 4, and KIEs on kinetic parameters are summarized in Table 4. For both the wild-type enzyme and H113A, values of $^{D}k_{cat}$ and $^{D}k_{cat}/K_m$ were greater than 1.00, indicating a significant normal isotope effect on the catalytic rates. Using kinetic parameters in Table 2 and KIEs in Table 4, eqs 5 and 6 could be employed to obtain estimates

Table 4: KIEs and S-KIEs on Kinetic Parameters for NADH-Dependent Xylose Reduction Catalyzed by Wild-Type CtXR and the H113A Mutant

enzyme	$^{D}k_{cat}$[a]	$^{D}k_{cat}/K_m$[a]	k_7[b] (s^{-1})	$K_{d\ Ald}$[c] (mM)	$^{D_2O}k_{cat}$[a]	$^{D_2O}k_{cat}/K_m$[a]
wild type	1.47 ± 0.10	2.50 ± 0.35	145	302	0.97 ± 0.05	0.91 ± 0.03
H113A	1.38 ± 0.06	1.61 ± 0.13	0.16	75	0.95 ± 0.03	0.93 ± 0.08

[a] From fits of initial rate measurements to eq 4; superscripts D and D_2O indicate primary deuterium and solvent deuterium kinetic isotope effects, respectively. [b] Calculated with eq 6 using data from this table and Table 2. [c] Calculated with eq 5 using data from this table and Table 2.

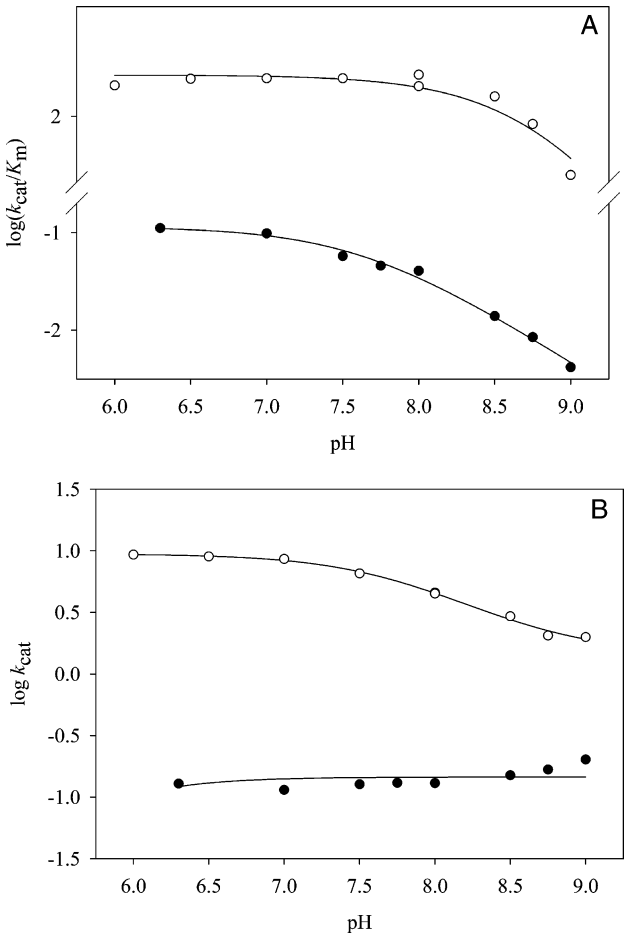

FIGURE 3: pH profiles of log($k_{cat}/K_{m\ xylose}$) (A) and log k_{cat} (B) for the NADH-dependent reduction of xylose catalyzed by wild-type CtXR (open circles) and the H113A mutant (filled circles). Lines represent fits of the data to the appropriate equation, as described in the text.

of the dissociation constant of the ternary complex $K_{d\ Ald}$ and the hydride transfer rate constant k_7, respectively. Comparison of calculated values shows that k_7 was slowed ≈1000-fold in the reaction catalyzed by the mutant, compared to the same reaction by the wild-type enzyme. By contrast, the effect of the mutation on $K_{d\ Ald}$ was small. We also determined $^{D}k_{cat}$ and $^{D}k_{cat}/K_m$ for the wild-type enzyme at pH 8.0 and 8.75. Values of $^{D}k_{cat}$ and $^{D}k_{cat}/K_m$ were constant within the limits of experimental error for the KIE (±5% for $^{D}k_{cat}$; ±15% for $^{D}k_{cat}/K_m$) as the pH was increased from 7.0 to 8.75.

Initial rate measurements were carried out in H_2O and D_2O solvent at pL 7.0, where L is H or D. They were performed under conditions in which the catalytic rates of the wild-type enzyme and H113A were pL-independent. Data recorded at varied [xylose] and constant [NADH] were fitted to eq 4, and S-KIEs are summarized in Table 4. Values of $^{D_2O}k_{cat}/K_m$ and $^{D_2O}k_{cat}$ for reactions catalyzed by the wild-type enzyme and H113A were smaller than 1.00, indicating an inverse S-KIE. The observed S-KIEs were on the borderline of significance considering the limits of detection in our experimental assays ($^{D_2O}k_{cat}$, ±3%; $^{D_2O}k_{cat}/K_m$, ±10%). However, it was clear that the wild-type enzyme and H113A did not differ in regard to S-KIEs on their kinetic parameters.

Table 5: Apparent Kinetic Parameters and KIEs for NADH-Dependent Reduction of 3X-BA Catalyzed by the H113A Mutant

3X-BA	k_{cat} (s^{-1})	k_{cat}/K_m ($M^{-1}\ s^{-1}$)	$^{D}k_{cat}$[a]	$^{D}k_{cat}/K_m$[a]	k_7[b] (s^{-1})	$K_{d\ Ald}$[c] (mM)
3-H	0.026	4.1	1.5[d]	2.0[e]	0.27	14
3-CH_3	0.014	11				
3-F	0.047	12	1.6[d]	1.7[e]	0.41	5.2
3-Cl	0.030	18				
3-Br	0.018	42				
3-CN	0.041	20	2.7[d]	2.1[e]	0.15	1.5
3-NO_2	0.024	850	2.1[d]	1.9[e]	0.08	0.025

[a] From fits to eq 4. [b] Calculated with eq 6 using data from this table. [c] Calculated with eq 5 using data from this table. [d] Standard errors were smaller than ±0.2. [e] Standard errors were smaller than ±0.3.

Structure−Activity Relationships for Reduction of Substituted Benzaldehydes by H113A. Initial rates of NADH-dependent reduction of 3X-BA by H113A were measured under conditions of varied [3X-BA] and constant [NADH] (230 μM). Kinetic parameters were obtained from fits of the data to eq 1 and are summarized in Table 5. Values of k_{cat}/K_m and k_{cat} showed a strong dependence on the variation of the substituent on the aromatic ring. A simple correlation of log(k_{cat}/K_m) or log k_{cat} with the electronic substituent parameter Hammett σ was nonlinear (not shown), indicating a complex substituent effect on the catalytic rates of H113A. Therefore, we assessed the substituent dependences of log(k_{cat}/K_m) and log k_{cat} in three-parameter correlations of the form:

$$\log(k_{cat}/K_m) \text{ or } \log k_{cat} = \rho\sigma + A\pi + BV_W \qquad (9)$$

where π is the Hansch hydrophobicity parameter, V_W is the molecular volume, and A and B are parameter coefficients. The data in Table 5 were fitted to eq 9, and results of multiple linear regression analysis are summarized in Table 6. r^2 values of ≥0.8 together with high F values (>6) at a significance level ($P = 0.09$) indicate a useful fit of eq 9 and the parameter coefficients shown in Table 6. The calculated electronic, hydrophobic, and steric substituent effects on log(k_{cat}/K_m) and log k_{cat} were significant statistically. Table 6 also shows a fit to eq 9 of k_{cat}/K_m values for 3X-BA reduction catalyzed by the wild-type enzyme.[2] Steric and bonding effects of the substituent on the H113A-catalyzed reaction were clearly lacking on the corresponding reaction of the wild-type enzyme. The value of $\rho(k_{cat}/K_m)$ measures the electronic substituent effect on the catalytic efficiency of 3X-BA reduction. It was strongly decreased in the reaction of the mutant, compared to the wild-type reaction

Table 6: Structure−Activity Relationship Analysis for Kinetic Parameters of NADH-Dependent Reductions of 3X-BA by H113A and the Wild-Type Enzyme

enzyme	kinetic parameter	σ^b	π^b	$V_W{}^b$	$r^{2\,c}$	F	P
H113A	k_{cat}/K_m ($M^{-1}\,s^{-1}$)[a]	0.78 ± 0.22	0.32 ± 0.09	0.32 ± 0.13	0.93	20.0	0.018
	k_{cat} (s^{-1})[a]	0.64 ± 0.23	-0.12 ± 0.09	-0.26 ± 0.14	0.81	6.2	0.086
wild type	k_{cat}/K_m ($M^{-1}\,s^{-1}$)[a]	1.67 ± 0.28	-0.06 ± 0.12	-0.11 ± 0.17	0.94	32.7	0.003

[a] From fits of the data to eq 9. [b] σ, π, and V_W are the electronic, hydrophobic, and steric (V_W) substituent parameters, respectively. [c] Coefficient of determination.

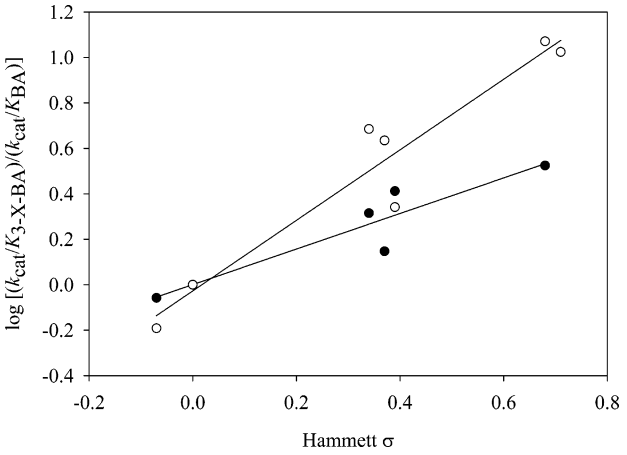

FIGURE 4: Hammett plot of the second-order rate constants for NADH-dependent reductions of 3X-BA catalyzed by wild-type CtXR (open circles) and the H113A mutant (filled circles). The k_{cat}/K_{3X-BA} values for H113A are corrected for hydrophobic and steric substituent effects, as shown in Table 5. Straight-line fits of the data are indicated, and results of regression analysis are shown.

in which the electronic effect was predominant. Furthermore, k_{cat} of the wild-type enzyme was devoid of any substituent effect (not shown). Figure 4 displays Hammett plots of the second-order rate constants of 3X-BA reduction by H113A and the wild-type enzyme.

We determined KIEs on k_{cat} and k_{cat}/K_m for H113A-catalyzed reduction of several 3X-BA substrates, as shown in Table 5. Equations 5 and 6 were used to obtain estimates for k_7 and $K_{d\,Ald}$ (Table 5). Both k_7 and $K_{d\,Ald}$ varied across the substrate series, but structure−activity relationship analysis of the substituent effect according to eq 9 was not attempted, considering a limited number of data points and experimental scatter of about ±20%.

DISCUSSION

H113A Holoenzyme Structure. Evidence from X-ray structure determination and ligand binding experiments indicates that the NAD(P) binding properties and the NADPH vs NADH specificity of wild-type CtXR are maintained in the H113A mutant. Therefore, this suggests that interpretations of the kinetic consequences of the mutation can be based on the assumption that the active site has not been globally disrupted by site-directed replacement of the original side chain with the side chain of alanine. The kinetic data are in excellent agreement with the X-ray structure of H113A-$NADP^+$, which reveals almost identical binding modes of cofactor in the wild-type enzyme and mutant holoenzymes.

The positions of most residues in the active site remain unchanged between wild-type CtXR and H113A; however, rotation of the Asp-50 carboxylate due to the loss of the histidine side chain displaces atoms as much as 3 Å. Modeling 3F-BA into the active site highlights the fact that this places the Asp-50 carboxylate approximately 3.5 Å from the predicted position of the substrate carbonyl. It is expected that this would inhibit a negative charge developing on the aldehyde oxygen in the transition state (see later).

Mutation of His-113 Slows the Hydride Transfer Step. Replacement of His-113 by alanine resulted in a marked loss of enzyme activity by a factor of about 1000, compared to the wild-type enzyme. The effect of the mutation was almost exclusively on the catalytic rate and not on apparent binding of coenzymes or substrates. This supports the notion that the main function of the side chain of His-113 is to facilitate the chemical reaction. The magnitude of the decrease in k_{cat} or k_{cat}/K_m for the mutant is consistent with a secondary role of His-113 in catalysis by CtXR (see later). KIEs on kinetic parameters for xylose reduction by the wild-type enzyme and H113A were used to estimate that hydride transfer (k_7) was slowed by ≈3 orders of magnitude as a consequence of the mutation. Employing the relationship $\Delta\Delta G^{\ddagger} = -RT \ln (k_{7\,H113A}/k_{7\,wild\ type})$, the decrease in k_7 for the mutant corresponds to a destabilization of the transition state of hydride transfer by about 16.9 kJ/mol.

Interpretation of KIEs. KIEs were diagnostic of major changes in the location of partly rate-limiting reaction steps caused by replacing His-113 by alanine. k_{cat}/K_m is a term that comprises all of the steps in the catalytic cycle from xylose binding to xylitol release. By contrast, k_{cat} includes also steps outside this part of the reaction sequence such as nucleotide exchange steps. During NADH-dependent reduction of xylose by the wild-type enzyme, the net rate of NAD^+ release is ≈90% rate-limiting for k_{cat} (*31*), reflected by $^Dk_{cat}$ being much smaller than $^Dk_{cat}/K_m$. In the case of H113A, the values of $^Dk_{cat}$ and $^Dk_{cat}/K_m$ are similar, which implies that the overall catalytic cycle is mainly rate-determining in the reaction of the mutant. The fact that the value of $^Dk_{cat}/K_m$ is smaller for H113A than the wild-type enzyme suggests that the observed isotope effects are controlled by different commitment factors (which are partition ratios for enzyme complexes that undergo the isotope-sensitive step in the forward and reverse directions). Now, because hydride transfer catalyzed by the mutant takes place at a slow rate, it is probable that $^Dk_{cat}/K_m$ for H113A represents the intrinsic isotope effect on k_7 [≈6.5 (*26*)] reduced only by internal commitments. A precatalytic equilibrium involving the xylose-bound enzyme may be responsible for a forward

[2] The structure−activity relationship analysis for NADH-dependent reduction of 3X-BA by wild-type CtXR has been reported elsewhere (*16*). However, to assess the kinetic consequences of replacing His-113 by alanine, we needed to determine kinetic data for the wild-type enzyme and H113A under exactly identical conditions. Results for the wild-type enzyme are in excellent agreement with the published data.

Scheme 1: Kinetic Mechanism of Xylose Reduction by Wild-Type Enzyme and H113A Involving a Precatalytic Isomerization of the Enzyme−NADH−Xylose Complex[a]

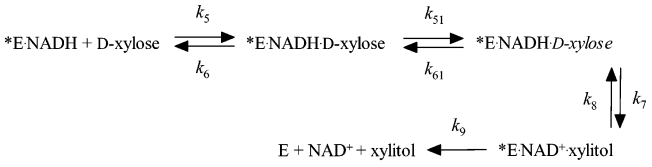

Isotope effect	Commitment factor
$^{D}k_{cat}/K_{xyl} = (^{D}k_7 + C_f + {}^{D}K_{eq}C_r)/(1 + C_f + C_r)$	$C_f = k_7/k_{61}(1+ k_{51}/k_6)$
$^{D}k_{cat} = (^{D}k_7 + C_{Vf} + {}^{D}K_{eq}C_r)/(1 + C_{Vf} + C_r)$	$C_r = k_8/k_9 << 1$
	$C_{Vf} \approx k_7(1/k_9 + 1/k'_{51})$

[a] All forward steps after formation of xylitol are comprised in k_9. k'_{51} is the net rate of the positioning step k_{51} and equals $(k_{51}k_7)/(k_7 + k_{61})$. $^{D}K_{eq}$ is the equilibrium isotope effect on the hydride transfer step. In the case of H113A, k_9 is expected to be much greater than k'_{51} and k_7.

commitment to catalysis (C_f), which has a substantial internal part ($C_{f-in} = k_7/k_{61}$, where k_{61} is the rate constant for the "off" isomerization of the ternary complex), as shown in Scheme 1.[3] Clearly, for C_{f-in} to have a high value in the reaction catalyzed by H113A, k_{61} must be smaller than k_7. In other words, replacement of His-113 by alanine seems to cause large decreases in the wild-type enzyme values for both rate constants k_{61} and k_7. Interpretation of KIEs for H113A-catalyzed reduction of 3X-BA by H113A corroborates the suggestion that mutation of His-113 strongly affects steps of an internal equilibrium prior to the hydride transfer step. KIE data for reductions of xylose and 3X-BA also imply that manifestation of the effect of the mutation is relatively independent of the structure of the nonreacting part of the aldehyde substrate.

Interpretation of pH Effects and Discussion of a Possible Role of His-113 in General Acid Catalysis by CtXR. Because the pH profiles of log k_{cat} may show pH dependences of steps outside the catalytic sequence, i.e., after xylitol has dissociated, we discuss first the pH profiles of log(k_{cat}/K_m). The pH profile of log(k_{cat}/K_m) for the wild-type enzyme shows an apparent pK_a of 8.85, above which the activity is lost. Therefore, because xylose does not ionize in the pH range studied, this indicates that a pH-sensitive group on the enzyme−NADH complex must be protonated for substrate binding and/or catalysis.[4] The pH profile of log(k_{cat}/K_m) for H113A displays a similar decrease at high pH above an apparent pK_a of 7.63, indicating a ΔpK_a of ≈ -1.2 pH units, compared to the corresponding pH profile of the wild-type enzyme, caused by the mutation. These data show clearly that the side chain of His-113 is not the ionizable group responsible for the pH dependence of log(k_{cat}/K_m) seen in the pH profile of the wild-type enzyme. If it were, the observed pK_a would be eliminated from the corresponding pH profile of the H113A mutant, irrespective of possible perturbations of pK_a values by substrate stickiness. However, there is of course the possibility that His-113 is involved in determining the apparent pK_a of another pH-sensitive group on the wild-type holoenzyme. A proximally disruptive nature of the mutation His → Ala could affect indirectly the pH-dependent ionization of this other enzyme group (see later).

The X-ray structure of H113A shows that the side chain of Asp-50 rotates to a position within 2.2 Å of the position occupied by the imidazole ring of His-113 in the wild-type enzyme. In H113A, there is a distance of ≈5 Å between the carboxylate of Asp-50 and the phenolic hydroxyl of Tyr-51, which according to structural considerations is a good candidate to which the experimental pK_a values in the pH profiles of log(k_{cat}/K_m) might be assigned, taking into account the possible perturbations by substrate stickiness. Previous studies of pH effects on AKR catalytic rates have assigned pK_a values on the basic limbs of pH profiles for k_{cat} (*4*, *5*) and k_{cat}/K_m (*6*, *7*) to tyrosines structurally equivalent to Tyr-51. However, we emphasize that our data do not per se support any pK_a-to-group assignment. Tyr-51 would be a structurally and functionally well-informed guess, also considering that there are a small number of residues in the catalytic site which ionize in the relevant pH range: Tyr-51; Lys-80 (not likely because the salt link interaction with the side chain of Asp-46 is expected to stabilize the protonated side chain of the lysine, thus elevating its pK_a); His-113 (pH effects on the reaction catalyzed by the H113A mutant rule out this possibility).

The distance between Nϵ2 of His-113 and Tyr-OH in the wild-type enzyme is ≈4 Å. This distance, compared with the distance of Tyr-51 and Asp-50 in H113A, is clearly too big to explain the observed ΔpK_a on account of differential hydrogen bonding. Interestingly, Lys-80 which interacts with Tyr-51 and Asp-46 in both wild-type and H113A holoenzyme structures experiences the greatest change in microenvironment as Asp-50 changes its conformation in the mutant. This may account for an indirect effect of the mutation on the protonation equilibrium of holo-CtXR, possibly involving Tyr-51.

These results are relevant mechanistically. A catalytic scenario for aldo−keto reductases has been proposed (*4*, *5*) in which a side-chain NH group of His-113 facilitates proton transfer from Tyr-51 by donating a hydrogen for bonding with the phenolic oxygen of the tyrosine. If exactly this mechanism of His-113 was operable in wild-type CtXR, one would expect that pH profiles of log(k_{cat}/K_m) for the H113A mutant are shifted to a significantly higher (not lower) value of apparent pK_a.

[3] The reverse commitment (k_8/k_9) is probably not significant in reactions catalyzed by the wild-type enzyme and H113A, considering that hydride transfer to NAD^+ occurs at a slow rate. Although the value of k_8 is not known exactly for H113A, we found no evidence that k_8 would be increased, compared to the rate constants of other steps of the catalytic cycle, as a result of the mutation. The ratio of k_{cat}/K_m values for xylose reduction and xylitol oxidation was not strongly affected by the mutation. In a previous study of the wild-type enzyme (*31*) we have shown that hydride transfer is partly rate-limiting for k_{cat}/K_m in both directions of the reaction.

[4] The observed pK_a of 8.85 in the pH profile of log(k_{cat}/K_m) for the wild type is apparent and may be perturbed from its correct position because xylose is slightly sticky. In the wild type, the stickiness ratio (S'_r), which is a ratio of the net rate constant of hydride transfer from NADH and the net rate constant of xylose release, has a value of ≈3.1 (*31*). Substrate stickiness may thus displace the apparent pK_a to a higher value by log($1 + S'_r$) (ΔpK_a = 0.61). The determination of a kinetically unperturbed value of pK_a by recording the pH profile of pK_i for a competitive inhibitor was not possible due to the lack of availability of an appropriate inhibitor. Likewise, we did not attempt to set up reaction conditions such that the catalytic step of aldehyde reduction is totally rate-limiting. A slow, thus nonsticky aldehyde substrate that would be more appropriate than xylose for detailed kinetic characterizations is not available for CtXR.

The pH profile of log k_{cat} for the wild type is a wave with an apparent pK_a of 7.80, in which log k_{cat} decreases from a constant value at the optimum pH of 6.0−7.0 to a lower constant value at pH ≈9.[5] Considering that log(k_{cat}/K_m) is not pH-dependent around pK_a 7.80, the pH profile of log k_{cat} may reflect the pH dependence of steps outside the catalytic cascade. To test this hypothesis, we determined the pH dependence of $^{D}k_{cat}$: if the rate of the noncatalytic step(s) decreased with increasing pH, the value of $^{D}k_{cat}$ should decrease above pK_a = 7.80. However, $^{D}k_{cat}$ was constant in the pH range 7.00−8.75. Therefore, this result implies that a group of pK_a 7.80, which is showing under conditions of saturation in xylose (k_{cat}) but is lacking when the xylose concentration is limiting (k_{cat}/K_m), must be protonated for an *optimum* catalytic rate; and the noncatalytic step which is partly rate-limiting for k_{cat} also decreases as the pH is increased above pK_a 7.80 so that the ratio of it and the chemical reaction remains constant. Obviously, these data suggest a conformational change in protein structure of the wild-type enzyme, which takes place as a result of xylose binding.

The k_{cat} of the H113A mutant is not pH-dependent in the pH range 6.0−9.0. Therefore, this implies that the pH-dependent ionization of a functional group in the H113A holoenzyme is completely masked at the level of the ternary complex (i.e., under substrate-saturated reaction conditions). Plausible explanations of this pH dependence are that xylose combines only with the protonated state of H113A-NADH, or binding to xylose partially locks the H113A holoenzyme in the correct protonation state for activity either by specific bonding interactions with the pH-sensitive enzyme group or by solvent exclusion from the active site.[6]

Summarizing, the pH profiles of log k_{cat} and log(k_{cat}/K_m) for the wild type and H113A do not suggest an important role of His-113 in general acid catalysis to carbonyl group reduction by CtXR. The absence of a solvent KIE on kinetic parameters for the mutant supports this notion, as follows. If His-113 were the actual proton donor of the reaction or facilitated proton donation from another group such as Tyr-51 (*4*, *5*), the replacement of His-113 would be expected to slow substantially the proton transfer step in the mutant. Now, irrespective of whether hydride transfer and proton transfer occurs in the same transition state or in different transition states, relatively slow catalytic proton transfer should be manifested in a sizable normal S-KIE on k_{cat} and k_{cat}/K_m for xylose reduction by H113A.[7]

No Evidence of Noncovalent Bonding of His-113 with the Substrate C2(R) Hydroxy Group. Previous studies of human aldose reductase (hAR; AKR 1B1), mammalian aldehyde reductase (AKR 1A1), and 3α-hydroxysteroid dehydrogenase (AKR 1C9) have shown that His-113 assists in orienting the substrate in the binding pocket. The finding of Bohren et al. (*6*) that His-113 determines the large stereochemical selectivity of hAR for *R*- over *S*-configured 2-hydroxyaldehydes was particularly relevant considering the close structural similarities among the physiological substrates of CtXR (xylose) and hAR (glucose). CtXR requires hydrogen-bonding interactions with the C2(*R*) hydroxy group to achieve full catalytic competence for reduction of 2-hydroxyaldehydes (*32*). We find that the H113A mutant prefers D-galactose over 2-deoxy-D-galactose as a substrate for NADH-dependent reduction to the same extent as the wild-type enzyme. This result can be interpreted to mean that the imidazole side chain of His-113 is not involved in the interactions with the 2-OH group of the substrate or that another group on the enzyme or perhaps water is capable of replacing it for noncovalent bonding in the H113A mutant. Modeling experiments in which a xylose molecule was docked into the active site of CtXR have suggested that the Nδ of Asn-309 is the most likely candidate to donate a hydrogen for bonding to the substrate C2(*R*) hydroxy group. The net loss of transition state stabilization energy of ≈7−8 kJ/mol in the reaction with the 2-deoxy-D-galactose, compared to reaction with D-galactose, would be consistent with the removal of a strong hydrogen bond between uncharged donor and acceptor groups. In the model of xylose binding, His-113 is not brought into position to serve as a candidate interaction partner with the 2-OH. Its Nϵ2, however, may be hydrogen-bonded with the carbonyl oxygen of the substrate (see later). In conclusion, we have found no evidence that His-113 contributes to a stabilization of the transition state of CtXR-catalyzed reduction of xylose by providing noncovalent interactions with the 2-OH.

Structure−Activity Relationships for Reduction of Aromatic Aldehydes by H113A. (A) Electronic Effects. The positive values of 0.78 and 0.64 for $\rho(k_{cat}/K_m)$ and $\rho(k_{cat})$, respectively, show that (1) electronic-withdrawing substituents speed the reaction of H113A with 3X-BA and (2) the electronic substituent effect on the enzymic rate is similar under conditions of limiting and saturating substrate concentration. $\rho(k_{cat}/K_m)$ for the wild type (=+1.7) is significantly greater than $\rho(k_{cat}/K_m)$ for H113A, revealing a substantially higher sensitivity of the wild-type enzyme catalytic efficiency to the electronic substituent effect. In the wild type, the hydride transfer rate constant k_7 is devoid of a substituent effect, electronic or otherwise (*16*). The proposed catalytic scenario for 3X-BA reduction by the wild type involves a substantial decrease in positive charge at the reactive carbon of the aldehyde upon moving along the reaction coordinate from the holoenzyme and free 3X-BA to the transition state (*16*). In contrast to the wild type, k_7 of

[5] We do not imply that the value of log k_{cat} of the wild type remains constant at pH values greater than 9. In fact, a significant perturbation of apparent pK_a seen in the pH profile of log(k_{cat}/K_m) is predicted for the pH profile of log k_{cat} because steps involved in NAD^+ release, rather than catalysis, are 90% rate-limiting (*31*). If the pK_a value of the log(k_{cat}/K_m) profile was thus shifted outward by the expected ≥1 pH units [=log(1 + 9)], the pK_a would escape detection in the log k_{cat} profile.

[6] The possibility that the pK_a seen in the log(k_{cat}/K_m) profile is perturbed in the log k_{cat} profile because of a change in rate-limiting steps is unlikely and not considered here. Release of NAD^+ is clearly not rate-limiting in the reaction catalyzed by H113A, as suggested by similar KIEs on k_{cat} and k_{cat}/K_m.

[7] The pL profile of log(k_{cat}/K_m) for the wild-type enzyme displays a plateau in the range pL 6.0−8.0 in H_2O or D_2O solvent. The observed S-KIE on k_{cat}/K_m is therefore real and does not reflect the difference in pL-dependent ionization of a functional enzyme group in H_2O and D_2O. If we consider (1) the pK_a of 7.63 in the pH profile log(k_{cat}/K_m) for H113A and (2) the fact that amino acid side chains are weaker acids in D_2O than H_2O, the ΔpK_a being ≈0.4−0.6 pH unit, a pL dependence of k_{cat}/K_m is expected for the mutant above pD 7.0. However, we emphasize that a sizable normal S-KIE on k_{cat}/K_m for H113A at pL 7.0 could not have escaped our detection: a pL-dependent ionization of the functional group of pK_a = 7.63 on the mutant may not differ by more than 10% in H_2O and D_2O solvent under these conditions.

H113A displays a significant dependence on the variation of the substituent on the aromatic ring. Obviously, the mutation causes an increased sensitivity of the catalytic step of hydride transfer to a substituent effect which may be complex and whose constituent electronic and bonding factors remain unresolved, however.

(B) Steric and Bonding Effects. Structure−activity relationship analysis of the substituent dependences of k_{cat} and k_{cat}/K_m for 3X-BA reduction by H113A has revealed the sensitivity of the mutant catalytic rates to changes in steric and hydrophobic characteristics of the substituent. By contrast, steric and bonding factors are lacking completely in the reaction of the wild type with the same series of substrates. Interestingly, the structural variations of the substituent do not have the same effects on k_{cat} and k_{cat}/K_m for H113A.

We have looked at how 3X-BA might bind in the active sites of the wild-type enzyme and H113A using modeling experiments. The docking studies show that 3F-BA can be positioned into the active site in two different orientations: one in which the fluorine is inserted into a cluster of hydrophobic residues composed of Trp-82, Phe-114, Phe-131, and Trp-314 and another in which the fluorine is directed toward the solvent (Figure 2). As the volume and polarity of the meta group are increased, we expect the latter conformation to be favored because steric conflicts would arise between the substituent and the hydrophobic pocket.

A Unified Role of His-113 in AKR Catalysis? Can the observations made herein and by others be reconciled in a unified mechanism of His-113 in catalysis to carbonyl group reduction by AKRs? We think that current AKR structures together with results from site-directed mutagenesis are consistent with a *major* function of His-113 in the precise positioning of the carbonyl group for catalysis. Additional roles such as H-bonding with nonreacting groups on the substrate (*6*, *8*, *11*) and fine-tuning of general acid−base catalysis (*4*, *5*, *11*) may occur in certain but obviously not all AKR members. In the mechanism we would like to propose, the Nϵ2 of His-113 is protonated in the ternary complex and acts as a hydrogen donor for bonding with O1 of the substrate.[8] The orbital interactions resulting from this conformation would direct a lone pair of electrons on O1 toward the phenolic proton of Tyr-51, enabling another strong hydrogen bond in the reactant state. The carbonyl group would thus be strongly polarized, making the C1 more electron-deficient overall and hence reactive for the nucleophilic attack by a hydride ion. The partial negative charge thus present on O1 would be stabilized by the interactions with Tyr-51 and His-113. We envision that the environment of the phenolic proton of Tyr-51 that is hydrogen-bonded to O1 will change synchronously as hydride transfer to C1 occurs and, consequently, the pK_a of O1 increases.[9] By contrast, the interactions between Nϵ2−H and O1 in the RCH═O reactant state and RCH_2OH product state are probably similar, which would explain why replacement of the imidazole side chain of His-113 by the methyl group of alanine leads to identical decreases in the forward and reverse catalytic rates of the mutant, compared to the wild-type enzyme. The suggested mechanistic scenario involves a trans addition of hydrogens to C1 and O1 with an (likely anti-coplanar) arrangement of the σ-type bond orbitals of C4−H of NADH and O−H of Tyr-51. In the productive complex, the π^* antibonding orbital of the carbonyl group (i.e., its lowest unoccupied molecular orbital) is expected to be positioned such that it points toward the C4−H bond orbital of NADH. The hydrogen bond donor group at His-113 would thus assist in optimizing both charge separation within the reactive carbonyl group (a Coulomb effect) and orbital alignment of nucleophile and substrate to facilitate the hydride transfer step (*34*). In the reverse reaction when xylitol is oxidized, a lone pair of electrons on O1 of the primary alcohol group is expected to delocalize into the antibonding σ^* orbital of the adjacent C1−H bond, thereby destabilizing this bond and facilitating hydride transfer to C4 of NAD^+. Again, positioning through bonding with His-113 will be important. Interestingly, a group of flavin-dependent oxidoreductases which are thought to operate by a hydride transfer catalytic mechanism (*35*−*38*) seem to make use of a conserved histidine in a way very similar to that proposed for CtXR.

Sequence changes partly explain why a seemingly incoherent picture is derived from characterizations of His-113 mutants of different AKRs. Phe-114 of CtXR is replaced by a tryptophan in hAR (*2*). The Nϵ1−H of this tryptophan donates a hydrogen for bonding with the carboxylate group on inhibitors bound with the enzyme−$NADP^+$ complex (*33*, *39*) and, according to modeling experiments, interacts with the 2-OH on aldehyde substrates (*13*). His-113 of hAR may thus form a bifurcated hydrogen bond with both carboxylate oxygens on inhibitors or with the oxygens at C1 and C2 of 2-hydroxyaldehydes. In this scenario, His-113 is positioned in the center of a network of hydrogen bonds that contributes to substrate binding and catalysis by hAR. However, a recent ultra-high-resolution structure (*33*) of an hAR−$NADP^+$−inhibitor complex reveals hydrogen bonds from Oη−H of Tyr-51 and Nϵ2−H of His-113 to one carboxylate oxygen of the inhibitor and from Nϵ1−H of Trp-114 to the other oxygen. The presence of Phe-114 in the yeast enzyme suggests that binding of 2-hydroxyaldehydes by CtXR and hAR must be different. In fact, mutation of Phe-114 into a tryptophan results in weakening (rather than improving) apparent binding of xylose by a factor of approximately 30 (R. Kratzer and B. Nidetzky, unpublished results).

ACKNOWLEDGMENT

We thank Drs. M. Klimacek and R. Griessler for help in preparing the H113A mutant.

SUPPORTING INFORMATION AVAILABLE

One figure showing the purification of the H113A mutant documented by SDS−PAGE. This material is available free of charge via the Internet at http://pubs.acs.org.

REFERENCES

1. Hyndman, D., Bauman, D. R., Heredia, V. V., and Penning, T. M. (2003) *Chem.-Biol. Interact. 143*−*144*, 621−631.

[8] Nδ1 is assumed to be unprotonated, in agreement with experimental and theoretical studies of the protonation state of His-113 in the active site of aldose reductase (*13*, *14*, *33*). Tautomerization of the neutral imidazole ring may be disfavored electrostatically (*33*).

[9] This does, however, not imply that hydride transfer and proton transfer will occur in a fully concerted (synchronous) fashion.

2. Jez, J. M., Bennett, M. J., Schlegel, B. P., Lewis, M., and Penning, T. M. (1997) *Biochem. J. 326*, 625−636.
3. Nidetzky, B., Mayr, P., Neuhauser, W., and Puchberger, M. (2001) *Chem.-Biol. Interact. 130*−*132*, 583−595.
4. Schlegel, B. P., Jez, J. M., and Penning, T. M. (1998) *Biochemistry 37*, 3538−3548.
5. Penning, T. M. (1999) *J. Steroid Biochem. Mol. Biol. 69*, 211−225.
6. Bohren, K. M., Grimshaw, C. E., Lai, C. J., Harrison, D. H., Ringe, D., Petsko, G. A., and Gabbay, K. H. (1994) *Biochemistry 33*, 2021−2032.
7. Grimshaw, C. E., Bohren, K. M., Lai, C.-J., and Gabbay, K. H. (1995) *Biochemistry 34*, 14374−14384.
8. Barski, O. A., Gabbay, K. H., Grimshaw, C. E., and Bohren, K. M. (1995) *Biochemistry 34*, 11264−11275.
9. Tarle, I., Borhani, D. W., Wilson, D. K., Quiocho, F. A., and Petrash, J. M. (1993) *J. Biol. Chem. 268*, 25687−25693.
10. Terada, T., Fujita, N., Sugihara, Y., Sato, R., Takagi, T., and Maeda, M. (2001) *Chem.-Biol. Interact. 130*−*132*, 833−845.
11. Jez, J. M., and Penning, T. M. (1998) *Biochemistry 37*, 9695−9703.
12. Klimacek, M., Szekely, M., Griessler, R., and Nidetzky, B. (2001) *FEBS Lett. 500*, 149−152.
13. De Winter, H. L., and von Itzstein, M. (1995) *Biochemistry 34*, 8299−8308.
14. Várnai, P., and Warshel, A. (2000) *J. Am. Chem. Soc. 122*, 3849−3860.
15. Lee, Y. S., Hodoscek, M., Kador, P. F., and Sugiyama, K. (2003) *Chem.-Biol. Interact. 143*−*144*, 307−316.
16. Mayr, P., and Nidetzky, B. (2002) *Biochem. J. 366*, 889−899.
17. Hemsley, A., Arnheim, N., Toney, M. D., Cortopassi, G., and Galas, D. J. (1989) *Nucleic Acids Res. 17*, 6545−6551.
18. Mayr, P., Brüggler, K., Kulbe, K. D., and Nidetzky, B. (2000) *J. Chromatogr. B 737*, 195−202.
19. Otwinowski, Z., and Minor, W. (1997) *Methods Enzymol. 276*, 307−326.
20. Gehlhaar, D. K., and Fogel, D. B. (1999) *Acta Crystallogr. D55*, 484−491.
21. Kavanagh, K. L., Klimacek, M., Nidetzky, B., and Wilson, D. K. (2002) *Biochemistry 41*, 8785−8795.
22. Jones, T. A., Zou, J.-Y., Cowan, S. W., and Kjeldgaard, M. (1991) *Acta Crystallogr. A47*, 110−119.
23. Brünger, A. T., Adams, P. D., Clore, G. M., DeLano, W. L., Gros, P., Grosse-Kunstleve, R. W., Jiang, J. S., Kuszewski, J., Nilges, M., Pannu, N. S., Read, R. J., Rice, L. M., Simonson, T., and Warren, G. L. (1998) *Acta Crystallogr. D54*, 905−921.
24. Klinman, J. P., and Matthews, R. G. (1985) *J. Am. Chem. Soc. 107*, 1058−1060.
25. Cook, P. F. (1991) Kinetic and regulatory mechanism of enzymes from isotope effects, in *Enzyme Mechanism From Isotope Effects* (Cook, P. F., Ed.) pp 203−230, CRC Press, Boca Raton, FL.
26. Grimshaw, C. E., Bohren, K. M., Lai, C.-J., and Gabbay, K. H. (1995) *Biochemistry 34*, 14356−14365.
27. Kraulis, P. J. (1991) *J. Appl. Crystallogr. 24*, 946−950.
28. Esnouf, R. M. (1997) *J. Mol. Graphics 15*, 113−138.
29. Merritt, E. A., and Bacon, D. J. (1997) *Methods Enzymol. 277*, 505−524.
30. Nicholls, A., Sharp, K. A., and Honig, B. (1991) *Proteins: Struct., Funct., Genet. 11*, 281−296.
31. Nidetzky, B., Klimacek, M., and Mayr, P. (2001) *Biochemistry 40*, 10371−10381.
32. Neuhauser, W., Haltrich, D., Kulbe, K. D., and Nidetzky, B. (1998) *Biochemistry 37*, 1116−1123.
33. Muzet, N., Guillot, B., Jelsch, C., Howard, E., and Lecomte, C. (2003) *Proc. Natl. Acad. Sci. U.S.A. 100*, 8742−8747.
34. Mesecar, A. D., Stoddard, B. L., and Koshland, D. E., Jr. (1997) *Science 277*, 202−206.
35. Lario, P. I., Sampson, N. S., and Vrielink, A. (2003) *J. Mol. Biol. 326*, 1635−1650.
36. Sampson, N. S., and Vrielink, A. (2003) *Acc. Chem. Res. 36*, 713−722.
37. Umhau, S., Pollegioni, L., Molla, G., Diederichs, K., Welte, W., Pilone, M. S., and Ghisla, S. (2000) *Proc. Natl. Acad. Sci. U.S.A. 97*, 12463−12468.
38. Zhao, G., Song, H., Chen, Z. W., Mathews, F. S., and Jorns, M. S. (2002) *Biochemistry 41*, 9751−9764.
39. Wilson, D. K., Tarle, I., Petrash, J. M., and Quiocho, F. A. (1993) *Proc. Natl. Acad. Sci. U.S.A. 90*, 9847−9851.

BI035833R